Rotational Flow in a Narrow Annular Gap Based on Lattice Boltzmann Method

*WANG Yimiao, ZHANG Jingyang, ZHU Guiping**

College of Astronautics, Nanjing University of Aeronautics and Astronautics, Nanjing 210016, P.R. China

(Received 27 March 2021; revised 23 May 2021; accepted 27 May 2021)

Abstract: For comprehensive characteristics of flow in a gas bearing, lattice Boltzmann method (LBM) is applied for study of the two-dimensional flow between two eccentric cylinders with the inner one rotating at a high speed. The flow pattern and circumferential pressure distribution are discussed based on critical issues such as eccentricity ranging from 0.2 to 0.9, clearance ratio varying from 0.005 to 0.01 and rotating speed in the range of 3×10^4—1.8×10^5 r/min. The analysis and discussion on the circumferential pressure distribution affirmed the quasilinear relation between the extremum pressure and rotating speed. Furthermore, a high eccentricity and small clearance ratio contributes most to the fluctuation of the circumferential pressure distribution. The flow pattern inside the channel exhibits separation vortex under a large eccentricity. The conclusions drawn in this work give rise to prediction of the flow pattern in the gas bearing which is beneficial for evaluating the performance of as well as instructing the design and development.

Key words: narrow annular; eccentric rotating cylinders; gas bearing; lattice Boltzmann method (LBM)

CLC number: TK05 **Document code:** A **Article ID:** 1005-1120(2021)03-0427-10

0 Introduction

In research, industrial, aeronautical fields etc., bearings are widely used and is of great importance for the performance of critical mechanical components[1]. Compared with conventional bearings, gas bearings are preferred with the advantages of oil free, non-pollution and so on. Its extraordinary performance that could operate at high-speed of more than 10^4 r/min brings itself many applications in the light-weights and high-speed machines[2-3]. The working mechanism of gas bearings, known as the hydrodynamic effect, is capacity formation for supporting of the rotor by pressure gradient generation with fluid passing through an unevenly channel. For this purpose, the magnitude of the clearance is minuscule, usually even less than 100 μm. Up to now, flow mechanism in such a narrow clearance has still been a puzzle, which strongly deserves further consideration. In addition, the flow in the channel significantly couples with heat transfer at high rotating speed and somehow affects the structure of bearing.

The study of flow in a narrow clearance between eccentric cylinders dates back to 1886, when Reynold pioneered the famous differential equations describing the pressure distribution in journal bearings. Henceforth, researchers[3] revealed that the solution of Reynold equations is an approximation to the Navier-Stokes (N-S) equations when it comes to a small clearance ratio. As a result, application of the Reynold equations is significantly developed in the study of journal bearings. The theory based on Reynold equations had been improved continuously and formed a comprehensive hierarchy. For example, Reynold equations were utilized to individually analyze the hydrodynamic effect in simplified wedge-shaped channels[4-6]. Furthermore, conditions in the whole annular were also discussed extensively. Thermohydrodynamic models that coupled the energy equation with Reynold equations were developed

*Corresponding author, E-mail address: zhuguiping@nuaa.edu.cn.

How to cite this article: WANG Yimiao, ZHANG Jingyang, ZHU Guiping. Rotational flow in a narrow annular gap based on lattice Boltzmann method[J]. Transactions of Nanjing University of Aeronautics and Astronautics, 2021, 38(3): 427-436.

http://dx.doi.org/10.16356/j.1005-1120.2021.03.007

to predict the temperature rise and pressure distribution of the air film[7-9]. Moreover, thermal structural effect[10-11] and cooling flow[12] were considered for further improvement of the results. Resulting in a lower capacity, the wall slip caused by gas rarefaction effect was proved to be nonnegligible at a high Knudsen number[13-14]. The aforementioned studies advance the gas bearing but focused little on the flow field of the air film, which are not accessible through Reynold equations.

The laminar flow between eccentric cylinders with one rotating wall has been widely discussed under large clearance ratio. Numerous methods have been applied to problems, such as finite element method[15], mixed Galerkin method[16], variational multiscale element free Galerkin method[17], direct simulation Monte Carlo approach[18], boundary element method[19], multigrid finite difference scheme[20] and boundary integral equation method[21]. Analytical solutions for Stokes flows between two infinitely long cylinder were given by Ballal et al.[22] with flow patterns investigated under different parameters. Separation vortex was generated when eccentricity of the channel exceeded a critical value. The positions where it started and ended, so called separation point and reattachment point, were independent of the speed of the inner cylinder and symmetrically located along the whole annular. The existence of the vortex was verified by experiments[23], in which the torque and flow force exerted on the cylinders were examined. Considering the inertial effect, Andres[24] analyzed how the flow pattern transformed at varying Reynolds number and eccentricity. Different from Stokes flow, the symmetry of the separation vortex no longer existed. Non-isothermal conditions were investigated with variable-viscosity by Dai et al[25]. The flow pattern was influenced by geometry as well as thermal boundary conditions. The stress patterns were studied with varying boundary conditions and eccentricities[26-27]. Taking rarefaction into account, gas flow between eccentric cylinders was investigated with outer cylinder rotating[18]. Under high Knudsen number, velocity slip induced by rarefaction was capable of suppressing the separation vortex mentioned above.

All the studies were conducted with a clearance ratio dozens of times larger than that of gas bearing. In other words, situations with extreme low clearance ratio still require extra exploration. However, conventional continuum models are unable to give an accurate solution once it comes to the hydraulic diameter less than 1 mm. LBM based on kinetic theory had better performance in the application of microscopic flow[28]. The movement of molecules is considered as cluster evolution, in which the molecules transfer and collide with each other, following energy and momentum conservation during collision. Most importantly, LBM's prominent computational efficiency makes it competent for micro scale computational study.

To sum up, the design of gas bearings still lacks of theoretical support, especially for the high-speed flow in the narrow annular configuration. The small-scale rotating flow gives rise to sophisticated field distribution and coupling effect, which is seldom reported. This work aims to examine the flow mechanism in a narrow annulus which stands for the clearance in gas bearings. The flow pattern and pressure distribution are obtained and discussed in terms of eccentricity, rotating speed and clearance ratio. As Reynolds number grows, the flow becomes unstable and a three-dimensional Taylor vortex appears[29]. The fundamental work presented here focuses on flow pattern at cross section and keeps the axial variation for further study and discussion.

1 Methods

For LBM, space is divided into a series of lattices that align with each other. The nodes on the lattices match the corresponding one on the adjacent lattice. Collision term in the equation is replaced by the Bhatnagar-Gross-Krook (BGK) operator. Thus, the Boltzmann equation can be described as

$$\frac{\partial f}{\partial t} + c \cdot \nabla f = \Omega \tag{1}$$

where f is the density distribution function, c the lattice velocity, and Ω the operator mentioned above. An approximation with a relaxation time τ and equi-

librium distribution function f^{eq} is used to describe the procedure during collision. Meantime, velocities of the lattices are discretized into several directions. The discrete Boltzmann equation without external force is

$$f_i(x+\Delta x,t+\Delta t)=f_i(x,t)+\frac{1}{\tau}[f_i^{eq}(x,t)-f_i(x,t)] \tag{2}$$

where i is the direction of particle velocity. The kinematical viscosity ν and relax time τ satisfy

$$\nu=\frac{(\tau-0.5)c^2}{3\delta t} \tag{3}$$

In the classic two-dimensional model (D2Q9), as shown in Fig.1, particle velocities are categorized into nine types.

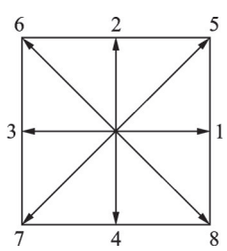

Fig.1 D2Q9 model

Accordingly, different particle velocity vectors can be written as

$$\boldsymbol{e}_i=\begin{cases}(0,0) & i=0\\ c\left[\cos\left[(i-1)\frac{\pi}{2}\right],\sin\left[(i-1)\frac{\pi}{2}\right]\right] & i=1,2,3,4\\ \sqrt{2}\,c\left[\cos\left[(2i-1)\frac{\pi}{4}\right],\sin\left[(2i-1)\frac{\pi}{4}\right]\right] & i=5,6,7,8\end{cases} \tag{4}$$

where the lattice velocity c is defined by $c=\delta_x/\delta_t$. δ_x is the length of lattice and δ_t is the time step. Thus, the equilibrium distribution is

$$f_i^{eq}=\omega_i\rho\left[1+\frac{3}{c^2}(\boldsymbol{e}_i\cdot\boldsymbol{u})+\frac{9}{2c^2}(\boldsymbol{e}_i\cdot\boldsymbol{u})^2-\frac{3}{2c^2}\boldsymbol{u}^2\right] \tag{5}$$

where ω_i is the weighting factor in each direction: $\omega_0=4/9$, $\omega_i=1/9(i=1,2,3,4)$, $\omega_i=1/36(i=5,6,7,8)$. Macroscopic parameters density ρ, velocity $\boldsymbol{u}$, and pressure p, can be calculated by

$$\rho=\sum_i f_i \tag{6}$$

$$\boldsymbol{u}=\frac{1}{\rho}\sum_i f_i\boldsymbol{e}_i \tag{7}$$

$$p=\frac{\rho c^2}{3} \tag{8}$$

The model of our calculation is shown in Fig.2.

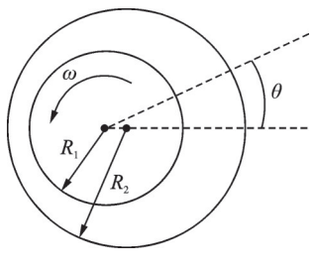

Fig.2 Annular channel as in journal bearing

We consider a rigid system with the shapes of the boundary remaining a circle. The rotor, with radius of R_1, rotates at a constant angular velocity ω in the counterclockwise direction. The parameter θ is circumferential degree that starts from the maximum thickness, with $\theta=180°$ corresponding to the minimum thickness. The radius of the outer boundary, R_2, equals to the radical clearance C plus the rotor radius R_1. Therefore, the clearance ratio c is

$$c=\frac{C}{R_1} \tag{9}$$

Reynolds number Re is defined as

$$Re=\frac{\omega R_1 C}{\nu} \tag{10}$$

Eccentricity ε is described by l, which is the distance between the centers of two circles

$$\varepsilon=\frac{l}{C} \tag{11}$$

The circumferential angle θ starts from the maximum clearance and varies from 0 to 2π following the rotating direction. Therefore, the local clearance is

$$h=C(1+\varepsilon\cos\theta) \tag{12}$$

Non-slip velocity boundary condition is assumed at both sides of the channel. The carved boundary is treated by the method described in Ref.[30]. As shown in Fig.3, the open circle ($\boldsymbol{r}_f$) and grey solid circle ($\boldsymbol{r}_b$) represent the nodes in fluid and solid region, respectively. The solid black circle ($\boldsymbol{r}_w$) indicates intersection of the node links and the dashed line, which is the real curved boundary.

Define q as

$$q=\frac{|\boldsymbol{r}_f-\boldsymbol{r}_w|}{|\boldsymbol{r}_f-\boldsymbol{r}_b|}\quad 0\leqslant q\leqslant 1 \tag{13}$$

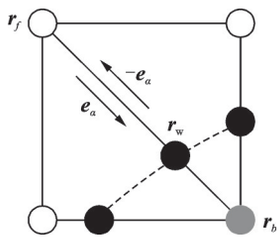

Fig.3 Method for curved boundary

The post-collision distribution function f^+ for node $\boldsymbol{r}_b$ can be written as

$$f_{\bar{\alpha}}^{+}(\boldsymbol{r}_b,t)=f_\alpha^{+}(\boldsymbol{r}_f,t)-\chi[f_\alpha^{+}(\boldsymbol{r}_f,t)-f_\alpha^{\mathrm{eq}}(\boldsymbol{r}_f,t)]+\omega_\alpha\rho(\boldsymbol{r}_f,t)\frac{3}{c^2}\boldsymbol{e}_\alpha[\chi(\boldsymbol{u}_{bf}-\boldsymbol{u}_f)-2\boldsymbol{u}_w] \tag{14}$$

$$\begin{cases}\boldsymbol{u}_{bf}=\boldsymbol{u}(\boldsymbol{r}_{ff},t),\chi=\dfrac{(2q-1)}{(\tau-2)} & 0\leqslant q<\dfrac{1}{2}\\ \boldsymbol{u}_{bf}=\dfrac{1}{2q}(2q-3)\boldsymbol{u}_f+\dfrac{3}{2q}\boldsymbol{u}_w,\chi=\dfrac{(2q-1)}{(\tau-1/2)} & \dfrac{1}{2}\leqslant q<1\end{cases} \tag{15}$$

where $\boldsymbol{e}_{\bar{\alpha}}=-\boldsymbol{e}_\alpha$, $\boldsymbol{r}_{ff}=\boldsymbol{r}_f+\boldsymbol{e}_{\bar{\alpha}}\delta t$ and $\boldsymbol{u}_f=\boldsymbol{u}(\boldsymbol{r}_f,t)$. Here $\boldsymbol{u}_w$ stands for the wall velocity, which is set to zero at the outer circle and the velocity of the rotor at inner circle, respectively. Owing to the negligible radial pressure gradient, the pressure at the center line of the thickness is taken as the typical results for the whole circumferential distribution. The working fluid is set as isothermal gas. Ambient pressure P_a is set to 0.1 MPa. Dimensionless pressure is described by

$$P_{\mathrm{non}}=\frac{P-P_a}{P} \tag{16}$$

The computational results are verified by comparing pressure distribution with data published by Diprima et al.[3] as shown in Fig.4. For comparison, the definition of pressure $(P-P_a)C^2/(\mu\omega R_1^2)$ is the same as the one employed in the above research with μ standing for the dynamic viscosity. The modified Reynolds number is 0.8 with eccentricity and clearance ratio at 0.75 and 0.08, respectively. The distribution in low pressure zone match well with each other and diverge slightly in the high pressure zone with discrepancy less than 6%. To conclude, the model constructed by utilizing LBM is accurate enough for calculating the annular flow.

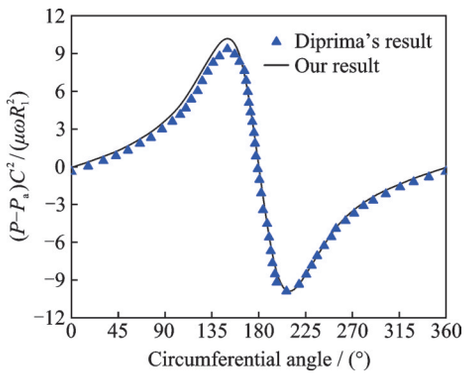

Fig.4 Verification of model by comparing with Diprima's result

2 Results

For a comprehensive understanding of the annular flow characteristics, the pressure and flow distribution are systematically studied in terms of the effect of eccentricity, rotor rotating speed and clearance ratio.

2.1 Effect of eccentricity

The distribution as well as the extremum of pressure are depicted in Figs.5, 6 with various eccentricities, while rotating speed and clearance ratio remain 3×10^4 r/min and 0.01, respectively. The Reynolds number is estimated to be 200. The increasing eccentricity gives rise to the absolute value of the maximum pressure and the minimum pressure. The circumferential pressure distribution fluctuates in a quite low level with eccentricity less than 0.4. The values of extremum pressure change smoothly with an increasing eccentricity smaller than 0.6, while upsurge significantly once eccentricity reaches 0.7. With a high eccentricity, the minimum thickness becomes smaller when the maximum thickness becomes larger on the contrary. Under the circumstance, the hydrodynamic effect will be more efficient, which brings dramatic changes in pressure distribution.

Furthermore, with eccentricity increasing from 0.2 to 0.9, the ratio of the maximum pressure to the minimum pressure keeps rising, ranging from 1.007 to 1.36. The maximum and minimum pressure appears at upstream of the minimum thickness ($\theta=180°$) and downstream of it, respectively. The positions of extremum pressure accord well with the lu-

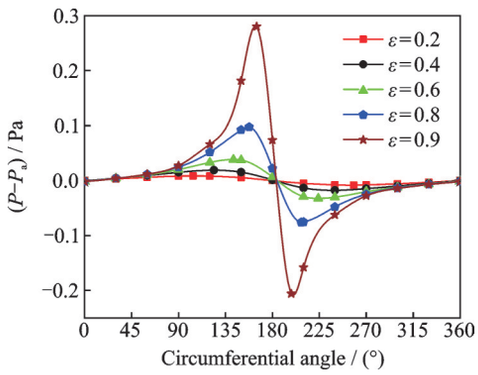

Fig.5 Non-dimensional circumferential pressure under different eccentricities

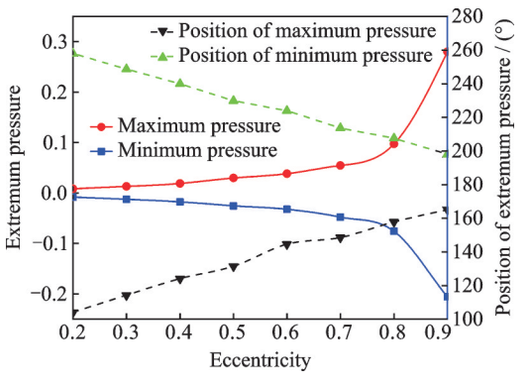

Fig.6 Value and position of extremum pressure

brication theory and approach the minimum thickness where a large pressure gradient is generated. In Fig.6, the two extremum pressure positions locate nearly symmetrically along the line of $y=180°$ and vary evenly with increasing eccentricity.

With eccentricity approximately reaches 0.4, back flow is generated in annular flow. This phenomenon is commonly studied in large clearance ratio and low Reynolds number condition. Henceforth, separation point and reattachment point are defined to describe the formation and distribution of the vortex. For example, in Ballal's results[22], the critical eccentricity was proved to be 0.324 24 with a clearance ratio of 0.5. For better understanding of back flow generation under extreme low clearance ratio, the streamline patterns are presented in Fig.7 at the eccentricity of 0.6. The typical images are shown with distribution at the maximum thickness, the separation and reattachment zones.

Upon generation, the vortex shifts along the channel and occupies the largest portion of the flow at the maximum thickness. The generation of separation vortex is caused by the existence of adverse pressure gradient along counterclockwise orientation. In a Stokes flow, the separation and reattachment points distribute symmetrically along the center line of the cylinders. In our study with Reynolds number larger than 200, both points A and C shift to the direction towards the minimum thickness of the annulus which is closer to the reattachment point. Fig.8 presents the positions of the separation point and reattachment point against eccentricity. As eccentricity ascends, the contraction and expansion of the annular become more drastic and thus induces a larger adverse pressure gradient and a wider clearance around the maximum thickness. As a result, the separation vortex is more likely to generate and occupies larger region in the channel, which can explain the approaching of points A and C.

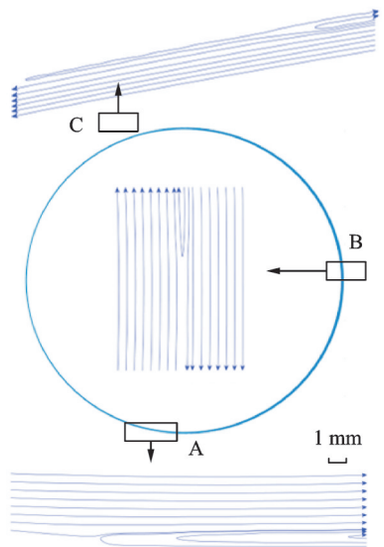

Fig.7 Diagram of positions A, B, C and the corresponding streamline

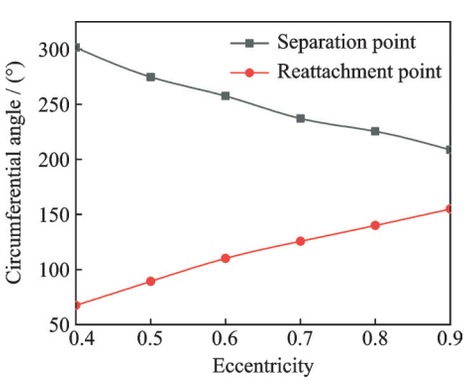

Fig.8 Positions of separate point and reattachment point against eccentricity

The tangential velocity, non-dimensionalized by $R_1\omega$, is shown in Figs. 9, 10, with distribution along the minimum and maximum thickness of the channel. Based on the analytical solution of a Couette flow, the variation of velocity is faster with a smaller favorable pressure gradient. Fig.5 demonstrates that minimum thickness suffers from favorable pressure gradient. With the eccentricity increasing from 0.2 to 0.5, the drops of tangential velocity from the rotor to the stationary boundary become slower along the minimum thickness. Upon exceeding the eccentricity value of 0.5, the variation rate of velocity no longer follows the pattern due to fluid compressibility, geometry change and the drastic pressure gradient change. The minimum thickness under eccentricity of 0.2 could be eight times as much as the one at the eccentricity of 0.9. Additionally, the difference of pressure gradient is significant according to Fig.5. Consequently, the coupling effects of pressure gradient and geometry contributes to the rate change of the velocity variation.

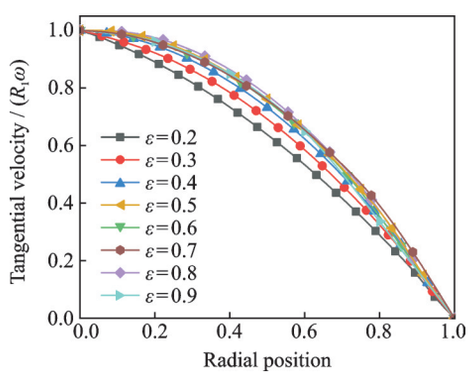

Fig.9 Non-dimensionalized tangential velocity along minimum thickness

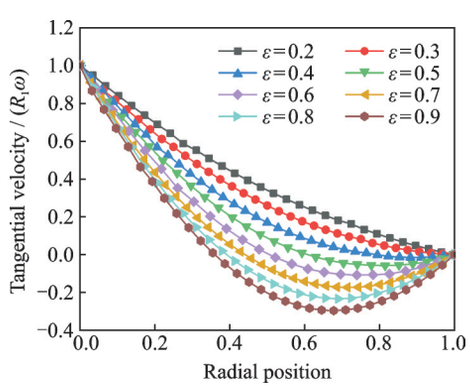

Fig.10 Non-dimensionalized tangential velocity along maximum thickness

In Fig.10, the non-dimensionalized tangential velocity gradually decreases from the rotor to the stationary boundary along the maximum thickness. The variation rate of the velocity becomes larger as the eccentricity increases due to the adverse pressure gradient. Negative velocity appears only when the eccentricity equals to or be greater than 0.4, corresponding to the back flow generation. As a result, the non-dimensionalized tangential velocity exhibits an increasing trend near to the stationary boundary with large eccentricity. In this region, the variation rate of the velocity also increases with eccentricity.

2.2 Effect of rotation speed

Fig.11 shows a comparison of pressure distributions with rotation speed increasing from 3×10^4 r/min to 1.8×10^5 r/min with an interval of 3×10^4 r/min. The calculation is implemented with clearance ratio and eccentricity fixed at 0.01 and 0.6, respectively. Both the absolute values of the maximum and minimum pressures increase almost linearly with the rotating speed, as shown in Fig.12. Posi-

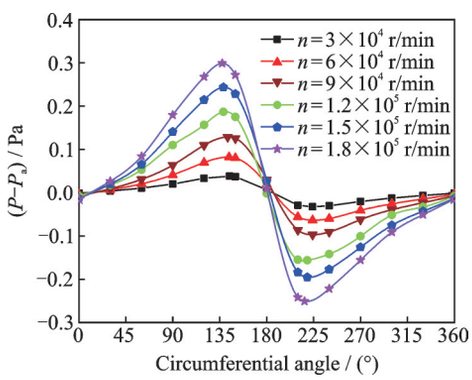

Fig.11 Non-dimensionalized pressure distribution under different rotating speeds

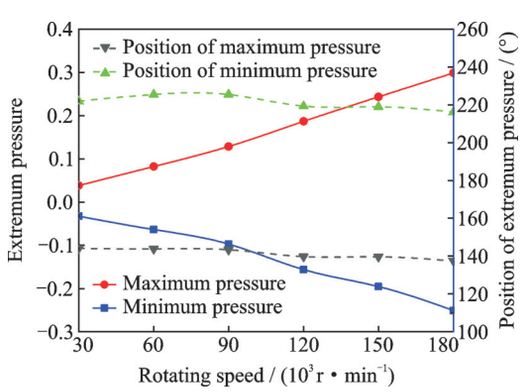

Fig.12 Value and position of extremum pressure

tions of both the maximum and the minimum pressures show no significant shift as rotating speed increases and mainly focuses within the area around 140° and 220°.

The non-dimensionalized tangential velocity along the minimum thickness and maximum thickness are shown in Figs.13, 14. At the minimum thickness, the non-dimensionalized tangential velocity is overall slightly higher with a larger rotating speed. At the region close to the rotor, the variation rate is larger at a lower rotating speed. As shown in Fig.14, the effect of rotor rotating speed seems negligible at the maximum thickness as the curves almost overlap with each other.

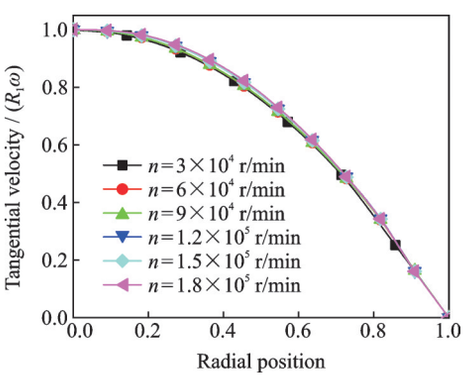

Fig.13 Non-dimensionalized tangential velocity along minimum thickness

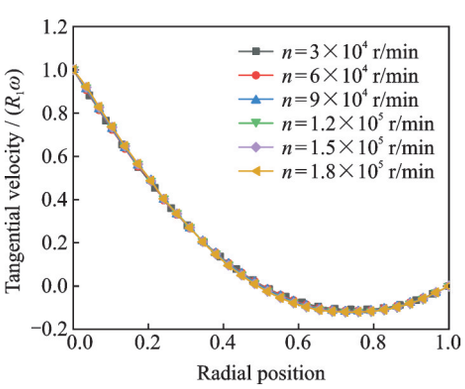

Fig.14 Non-dimensionalized tangential velocity along maximum thickness

The dependence of the positions of separation and reattachment point on the rotating speed is shown in Fig.15. The variation is confined in a range no more than 5 degree, indicating a negligible effect of the rotating speed on the location of the separation vortex. The reattachment point is about 10° closer to the minimum thickness than the separation point. For flow in small-scale channel with Reynolds number no less than 200 in this paper, the positions of separation and reattachment points almost remain stationary.

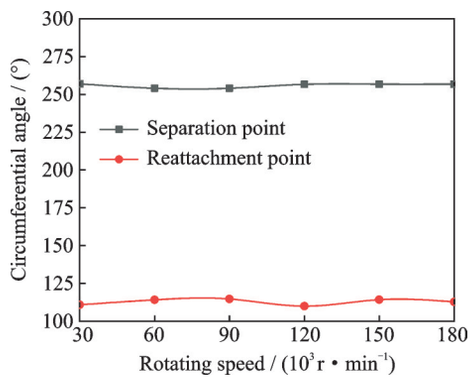

Fig.15 Positions of separation point and reattachment point against eccentricity

2.3 Effect of clearance ratio

Fig.16 depicts the pressure distributions when clearance ratios vary from 0.005 to 0.01. The rotating speed and eccentricity are set to 3×10^4 r/min and 0.6, respectively. Obviously, the value of extremum pressure decreases as clearance expands. Upon reaching 0.008, there is no significant variation of the extremum pressure in terms of the clearance ratio, as shown in Fig.17. To sum up, a narrower channel leads to a larger extremum of pressures. The variation of the separation and reattachment point positions are confined in a relatively small range, indicating negligible effect of the clearance ratio.

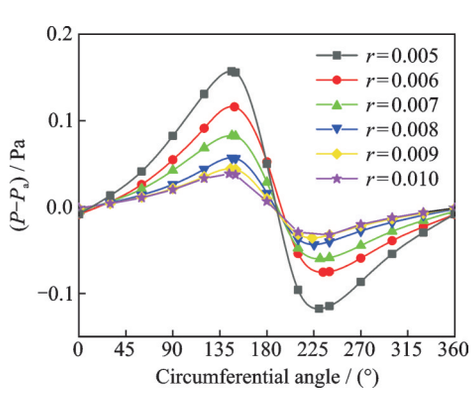

Fig.16 Non-dimensionalized pressure distribution under different clearance ratios

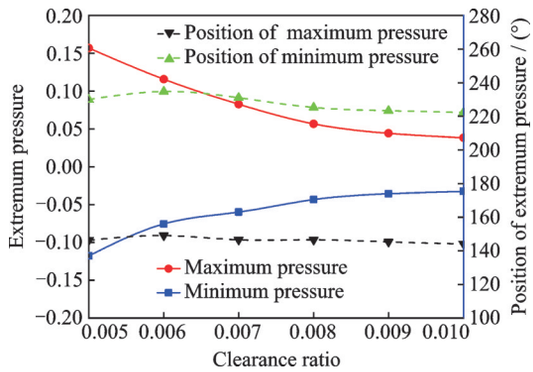

Fig.17 Value and position of extremum pressure

The velocity distribution along the minimum thickness is quite obscure, as shown in Fig.18. With the same rotating speed, the increase of clearance ratio could result in the expansion of the local clearances. Besides, the compressibility of the working gas and nonlinear relation between pressure and clearance ratio could contribute to other sophisticated factors.

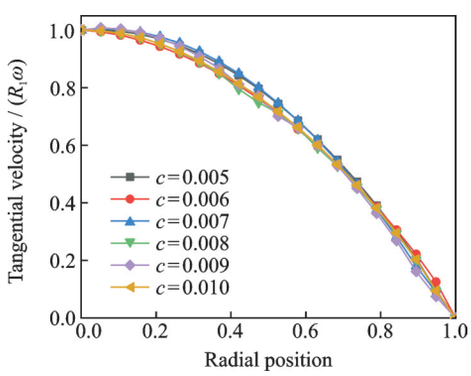

Fig.18 Non-dimensionalized tangential velocity along the minimum thickness

The distribution of non-dimensionalized tangential velocity along the maximum thickness of the channel is shown in Fig.19 at different clearance ratios. The extremum increases with enhancement of the clearance ratio. Overall, there is no tremendous variation of non-dimensionalized tangential velocity along the minimum and maximum thicknesses with clearance ratio varying. In Fig.20, the separation and reattachment points also remain almost stationary, indicating that the effect of clearance ratio is negligible.

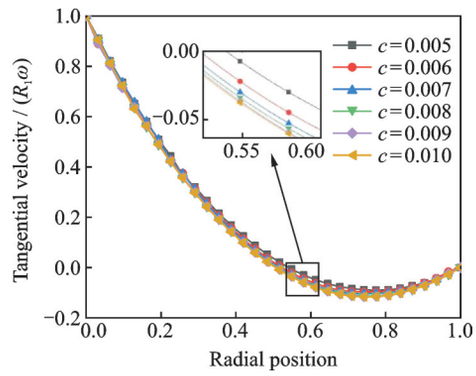

Fig.19 Non-dimensionalized tangential velocity along maximum thickness

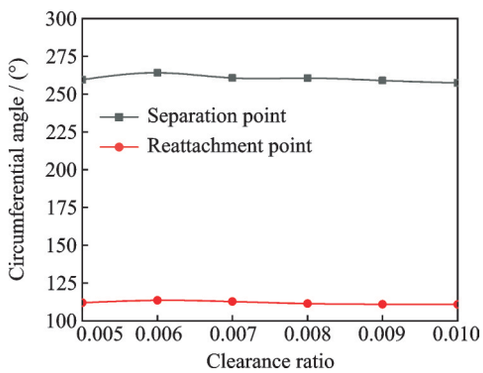

Fig.20 Positions of separation point and reattachment point against clearance ratio

3 Conclusions

The two-dimensional flow between eccentric cylinders with clearance ratio less than 0.01 is discussed. The pressure distribution and flow pattern are analyzed in terms of clearance ratio, rotation speed and eccentricity. Large eccentricity, high rotating speed and low clearance ratio can generate a drastically fluctuating pressure distribution. Furthermore, the extremum pressure is almost proportional to the rotating speed and upsurge significantly with eccentricity larger than 0.7 or clearance ratio smaller than 0.008. Meantime, the existence of an eccentricity-dependent separation vortex is affirmed with eccentricity exceed a critical value lying between 0.3 and 0.4. Eccentricity contributes mostly to the positions of extremum pressure and separation vortex. Considering the coupling effects of the pressure gradient and geometry, non-dimensionalized tangential velocity distributions are parametrically analyzed along the maximum and minimum thicknesses.

References

[1] LYU Yangming, WANG Zhongwang, WANG Hao, et al. Preload method based on waveform spring for angular contact bearing of space actuator[J]. Journal of Nanjing University of Aeronautics & Astronautics, 2018, 50(2): 34-38. (in Chinese)

[2] SALEHI M, SWANSON E, HESHMAT H. Thermal features of compliant foil bearings: Theory and experiments[J]. Journal of Tribology, 2001, 123(3): 566-571.

[3] DIPRIMA R C, STUART J T. Flow between eccentric rotating cylinders[J]. Journal of Tribology, 1971, 94(3): 266-274.

[4] DONG J S, SEO D K, SCHULTZ W W. A comparison study between Navier-Stokes equation and Reynolds equation in lubricating flow regime[J]. KSME International Journal, 2003, 17(4): 599-605.

[5] ZHANG X, CHEN Q, LIU J. Hydrodynamic behaviors of the gas-lubricated film in wedge-shaped microchannel[J]. Journal of Tribology, 2016, 138(3): 031701-031710.

[6] SNECK H J. An approximate solution for the infinitely long, gas lubricated slider bearing[J]. Journal of Fluids Engineering, 1965, 87(4): 1085-1086.

[7] PENG Z C, KHONSARI M M. A thermohydrodynamic analysis of foil journal bearings[J]. Journal of Tribology, 2006, 128(3): 534-541.

[8] WANG X F, GAO T C. Pressure angle effect of concave cylinder surface on motion characteristics of fiber placement machine[J]. Transactions of Nanjing University of Aeronautics and Astronautics, 2020, 37(6): 898-902.

[9] PAULSEN B T, MOROSI S, SANTOS I F. Static, dynamic, and thermal properties of compressible fluid film journal bearings[J]. Tribology Transactions, 2011, 54(2): 282-299.

[10] TALMAGE G, CARPINO M. Thermal structural effects in a gas-lubricated foil journal bearing[J]. Tribology Transactions, 2011, 54(5): 701-713.

[11] LEE D, KIM D. Thermohydrodynamic analyses of bump air foil bearings with detailed thermal model of foil structures and rotor[J]. Journal of Tribology, 2010, 132(2):16-22.

[12] LEE D, LIM H, CHOI B, et al. Thermal behavior of radial foil bearings supporting an oil-free gas turbine: Design of the cooling flow passage and modeling of the thermal system[J]. Journal of Engineering for Gas Turbines & Power, 2017, 139(6): 061902-061910.

[13] ZHANG H J, ZHU C S, MING T. Effects of rarefaction on the characteristics of micro gas journal bearings[J]. Journal of Zhejiang University A, 2010(1): 43-49.

[14] ZHANG W M, ZHOU J B, MENG G. Performance and stability analysis of gas-lubricated journal bearings in MEMS[J]. Tribology International, 2011, 44(7/8): 887-897.

[15] ARAUJO J, RUAS V, VARGAS A S. Finite element solution of flow between eccentric cylinders with viscous dissipation[J]. International Journal for Numerical Methods in Fluids, 1990, 11(6): 849-865.

[16] KIM E. A mixed Galerkin method for computing the flow between eccentric rotating cylinders[J]. International Journal for Numerical Methods in Fluids, 1998, 26(8): 877-885.

[17] ZHANG P, ZHANG X. Numerical modeling of Stokes flow in a circular cavity by variational multiscale element free Galerkin method[J]. Mathematical Problems in Engineering, 2014(1): 451546.

[18] SOCIO L M D, MARINO L. Numerical experiments on the gas flow between eccentric rotating cylinders[J]. International Journal for Numerical Methods in Fluids, 2000, 34(3): 229-240.

[19] TELESZEWSKI T J. Effect of viscous dissipation in Stokes flow between rotating cylinders using BEM[J]. International Journal of Numerical Methods for Heat & Fluid Flow, 2019, 30(4): 2121-2136.

[20] CHOU M H. A multigrid finite difference approach to steady flow between eccentric rotating cylinders[J]. International Journal for Numerical Methods in Fluids, 2000, 34(6): 479-494.

[21] RAMESH P S, LEAN M H. A boundary integral equation method for Navier-Stokes equations: Application to flow in annulus of eccentric cylinders[J]. International Journal for Numerical Methods in Fluids, 2010, 13(3): 355-369.

[22] BALLAL B Y, RIVLIN R S. Flow of a Newtonian fluid between eccentric rotating cylinders[J]. Archive for Rational Mechanics and Analysis, 1976, 62(3): 237-294.

[23] SUEMATSU Y, ITO T, MUKAI R. Two dimensional flow between eccentric rotating cylinders[J]. Bulletin of the JSME, 2008, 24(197): 1928-1937.

[24] ANDRES A S, SZERI A Z. Flow between eccentric rotating cylinders[J]. Journal of Applied Mechanics, 1984, 51(4): 869-878.

[25] DAI R X, DONG Q, SZERI A Z. Flow of variable-viscosity fluid between eccentric rotating cylinders[J].

International Journal of Non-linear Mechanics, 1992, 27(3): 367-389.

[26] BERIS A N, ARMSTRONG R C, BROWN R A. Finite element calculation of viscoelastic flow in a journal bearing: Ⅱ. Moderate eccentricity[J]. Journal of Non-Newtonian Fluid Mechanics, 1986, 19(3): 323-347.

[27] CHUN L R, LI W. Numerical study of viscoelastic flow between eccentrically rotating cylinders[C]//Proceedings of the 2012 International Conference on Advanced Mechatronic Systems. Tokyo, Japan: IEEE, 2012.

[28] JEONG N, LIN C L, CHOI D H. Lattice Boltzmann study of three-dimensional gas microchannel flows[J]. Journal of Micromechanics & Microengineering, 2006, 16(9): 1749-1759.

[29] OIKAWA M, KARASUDANI T, FUNAKOSHI M. Stability of flow between eccentric rotating cylinders[J]. Journal of the Physical Society of Japan, 2007, 58(7): 2355-2364.

[30] YAN Y Y, ZU Y Q. Numerical simulation of heat transfer and fluid flow past a rotating isothermal cylinder: A LBM approach[J]. International Journal of Heat & Mass Transfer, 2008, 51(9/10): 2519-2536.

Acknowledgement This work was partially supported by the Aeronautical Science Foundation of China (No. 201928052008).

Authors Mr. **WANG Yimiao** received his B.S. degree in flight vehicle design from College of Astronautics in Nanjing University of Aeronautics and Astronautics (NUAA) in 2019 and is currently pursuing his M.S. degree in NUAA, mainly focusing on engineering thermodynamics and computational fluid dynamics.

Dr. **ZHU Guiping** received her Ph.D. degree from mechanical engineering department of Nanyang Technological University in 2014. She has been awarded as "Innovation and Entrepreneurship Doctor" in the category of world famous university of the "Innovation and Entrepreneurship Program" of Jiangsu Province. She is mainly engaged in the research of micro magnetohydrodynamics and MHD, committed to digital magnetic microfluidics, power generation, propulsion based on MHD and its application in aerospace.

Author contributions Mr. **WANG Yimiao** conducted the computation and analysis, interpreted the results and wrote the manuscript. Dr. **ZHANG Jingyang** contributed to the discussion and background of the study, and revised the draft. Dr. **ZHU Guiping** designed the study, contributed to the discussion of the study, and proofread the manuscript. All authors commented on the manuscript draft and approved the submission.

Competing interests The authors declare no competing interests.

(Production Editor: ZHANG Tong)

格子Boltzman方法的微间隙旋转流动研究

王一淼，张镜洋，朱桂平

(南京航空航天大学航天学院,南京 210016,中国)

摘要:为了全面了解动压轴承的内部流动特性,使用了格子玻尔兹曼方法对内壁高速旋转的圆环间隙内的二维流动进行研究,在偏心率0.2~0.9,间隙比0.005~0.01,转速3×10^4~1.8×10^5 r/min的范围内讨论了流动和压力周向分布。通过研究发现,内壁的转速与压力极值的大小几乎成线性关系,而大偏心率和小间隙比则会带来压力分布的强烈变化。同时结果显示,在偏心率较大时流场中会出现分离涡。本文对气体轴承内部流动特性的分析有助于分析动压轴承的性能,并为其设计和改进提供指导。

关键词:微小间隙;偏心旋转的圆柱;气体轴承;格子玻尔兹曼方法